Pergamon

J. Mech. Phys. Solids, Vol. 42, No. 7, pp. 1067–1085, 1994

0022–5096/94 $7.00+0.00

0022–5096(94)E0020–5

HYDROSTATIC COMPACTION OF CYLINDRICAL PARTICLES

A. R. AKISANYA, A. C. F. COCKS and N. A. FLECK

Engineering Department, Cambridge University, Trumpington Street, Cambridge CB2 1PZ, U.K.

(*Received* 20 *October* 1993; *in revised form* 3 *March* 1994)

ABSTRACT

THE EFFECT OF particle contact–contact interaction and pore geometry is studied for the pressure–density relationship of powders undergoing hydrostatic compaction. The study is restricted to a two-dimensional array of cylindrical particles. Slip-line field theory is used to analyse the rigid–perfectly plastic response and the finite element method is used to explore the effect of material strain hardening. For both material descriptions, contact–contact interaction has a strong influence on the compaction process beyond the initial stage. The theoretical predictions are compared with experimental results for hydrostatic compaction of plasticene cylinders.

1. INTRODUCTION

1.1. *Industrial perspective*

CONSOLIDATED METAL POWDERS are finding increased use in engineering components due to the advantages which they offer in terms of mechanical properties and ease of processing. For example, complex shaped components such as gears and cams for automotive applications can be formed by pressing the powder in a suitably shaped die. After this stage of the process, the particles are weakly bonded together and the component is heated to an elevated temperature in a reducing atmosphere, allowing the particles to bond together. Because of their high strength, intermetallic and ceramic components are commonly manufactured using a powder route. Densification of the compact is achieved at elevated temperature with or without the simultaneous application of pressure.

In any manufacturing process it is important to be able to optimize the procedures to minimize the cost of production and maximize the reliability of the finished component. Currently, the process variables are largely determined in an *ad hoc* manner, based on experience of what has worked in the past. Computational simulation of compaction would considerably ease this process, but before this can be achieved appropriate constitutive laws for the powder response need to be developed.

1.2. *Densification mechanisms*

The densification of powder compacts involves various mechanisms: plastic flow, creep, diffusion and so forth. The densification rate is the superposition of the con-

tribution from all operating mechanisms. The effects of creep and diffusion are small at low homologous temperature; plastic flow becomes the dominant mechanism by which densification occurs under this condition. Also, plastic flow is the dominant mechanism of deformation in the early stages of compaction during hot pressing and hot isostatic pressing (HIPing). In this paper we are concerned with the densification of powders by plastic flow and leave the other mechanisms (creep and diffusion) for later treatment.

It is possible to identify two distinct stages of the compaction process of spherical powders. During the early stages of densification (stage I) the body contains a network of open porosity, with distinct necks between the particles. As densification proceeds the pores pinch-off leaving a network of isolated pores within the body. The subsequent response is generally referred to as stage II densification. In the current paper we examine the response of a two-dimensional array of cylinders, where the pores always lie along the axes of the cylinders. The above physical distinction of stages I and II is no longer appropriate, but it still proves convenient to separate the response into two different stages, where now each stage is characterized by the nature of the slip-line field solution that develops within the particles, assuming a rigid, perfectly plastic response.

Existing models (KAKAR and CHAKLADER, 1967; ARZT, 1982; SWINKEL *et al.*, 1983; HELLE *et al.*, 1985; ASHBY, 1990) for the pressure densification of powders by plastic flow during stage I are based on isolated contacts between the particles and on the increase of the number of such contacts. The plastic deformation zone is assumed to be localized around each contact, and there is no interaction between neighbouring deformation zones. The isolated contact model (ASHBY, 1990) assumes that the mean pressure on each particle contact is equal to the fully constrained Prandtl punch value of $P_{\text{eff}} = 2k(1+\pi/2)$ (HILL, 1950), where k is the shear yield strength of the material composing the powder particles (P_{eff} is the load on a contact divided by the contact area). Material models for stage II are based on idealizing each of the pores as an independent spherical void surrounded by a spherical shell of material. This idealization of the porosity in stage II is only valid if surface diffusion is sufficiently rapid for the pores to adopt an equilibrium shape throughout the deformation process. In cold compaction of powders (and in the early stages of hot isostatic pressing), the contribution from diffusion is negligible, and the pores remain cusped (LIU *et al.*, 1993). Thus, the isolated spherical void model is not appropriate in these instances.

1.3. *The role of particle contact–contact interaction*

The isolated contact model in stage I neglects the details of the particle geometry and also the possible interaction of the deformation zones emanating from each contact. The interaction of the deformation zones may occur early during densification, and thus render the isolated contact model invalid. Furthermore, the finite particle geometry imposes an upper limit on the ratio of contact size to particle radius for which the mean contact pressure in stage I equals the fully constrained Prandtl value.

The interaction of the deformation zone emanating from a contact with another deformation zone can lead to softening, where the local indentation pressure drops

below the Prandtl value. This is exemplified in Fig. 1, for the representative case of two opposite contacts, each of width $2x$ and a distance $2H$ apart. Interaction of the plastic zones occurs when $x/H > 0.1$. Softening is not always observed, however; interaction can sometimes lead to a hardening of the system response. We can demonstrate this effect by considering, for example, the row of indenters of width $2x$ and a distance $2H$ apart, as shown in Fig. 2(a). If $x < H$, then Hill's fully constrained slip-line field can develop under the indenters and $P_{\text{eff}} = 2k(1+\pi/2)$. As the indenters get closer together, the material squeezed out from under the indenters is forced to extrude up through an ever decreasing gap between the indenters, increasing the constraint on the deformation process. This leads to an increase in the value of P_{eff} required to drive the deformation process as demonstrated in Fig. 2(b).

It is evident from the above discussion that models that account for particle contact–contact interaction are required to predict accurately the densification pressure for powder compaction.

1.4. *Statement of the problem*

In this paper we investigate the effect of particle contact–contact interaction and of pore geometry upon the densification of powders. As a preliminary investigation, we evaluate the response of an idealized two-dimensional array of cylindrical particles. The compaction of two-dimensional particles is of practical importance in the manufacture of fibre-reinforced composites where both the fibre and the matrix can be cylindrical in geometry. Moreover, a two-dimensional model provides a useful, sim-

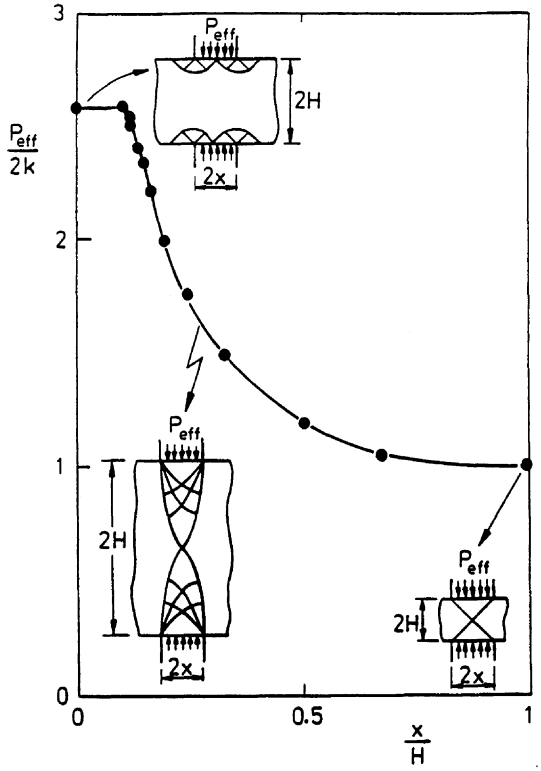

FIG. 1. Effect of finite particle geometry on the mean contact pressure for a particle with two opposing contacts. P_{eff} is the mean contact pressure, k is the shear yield strength of the particle, $2x$ is the contact size and $2H$ is the contact–contact distance. The inserts show the slip lines for the different modes of deformation.

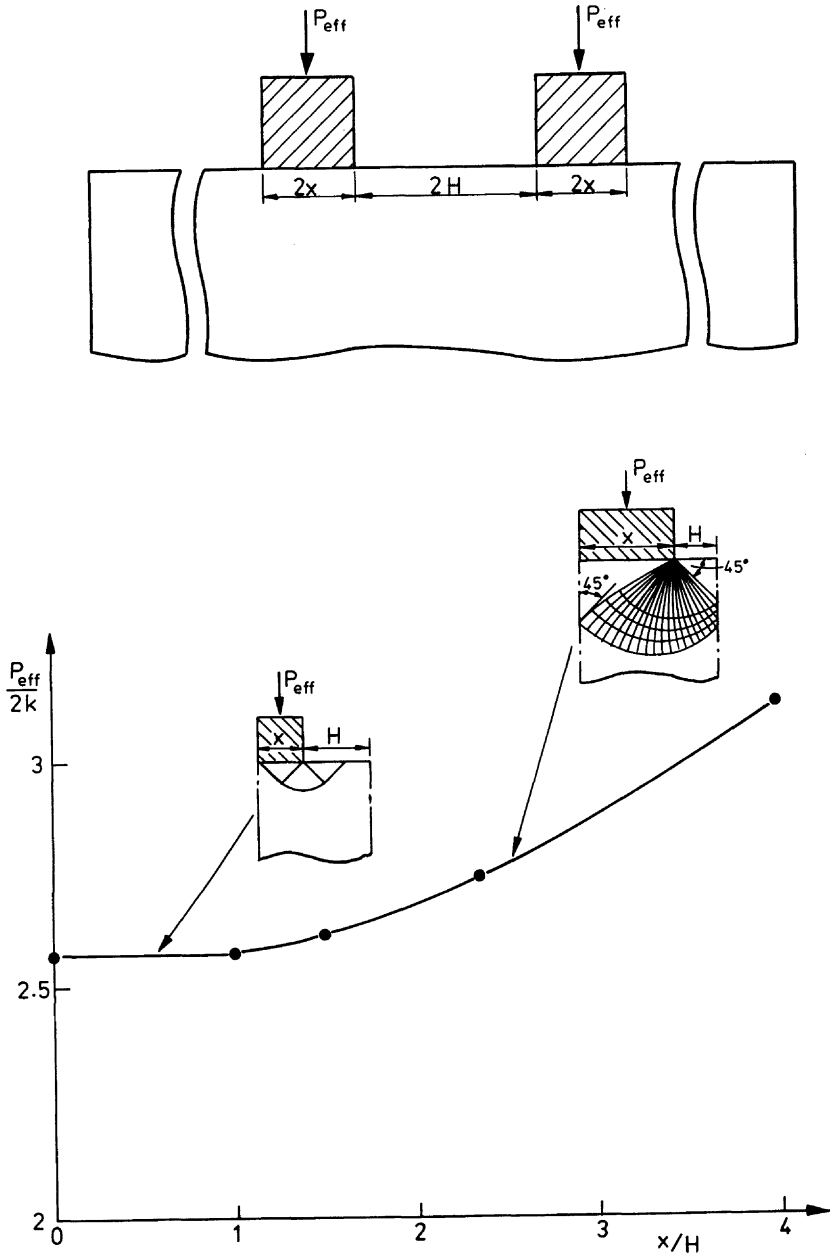

FIG. 2. The hardening response for an array of indenters due to contact–contact interaction.

plified way of examining the main aspects of the densification of spherical and other three-dimensional particles, such as the interaction between particle contacts.

The densification of cylindrical particles by creep and/or diffusion has been considered by various authors (MATSUMURA, 1971 ; SWINKEL and ASHBY, 1981 ; WILLIAMSON *et al.*, 1992). In the present study, we focus on the densification of cylindrical particles by rate independent plasticity. We consider the plane strain compaction of a hexagonal array of circular cylinders subjected to a macroscopic hydrostatic pressure P_{ex}, as shown in Fig. 3. The pressure versus density response for the array is determined using plane strain slip-line field theory for a rigid–perfectly plastic solid. The effect of material strain hardening upon densification is explored using a finite element analysis. Experimental results are presented for the hydrostatic compaction of plasticene rods ;

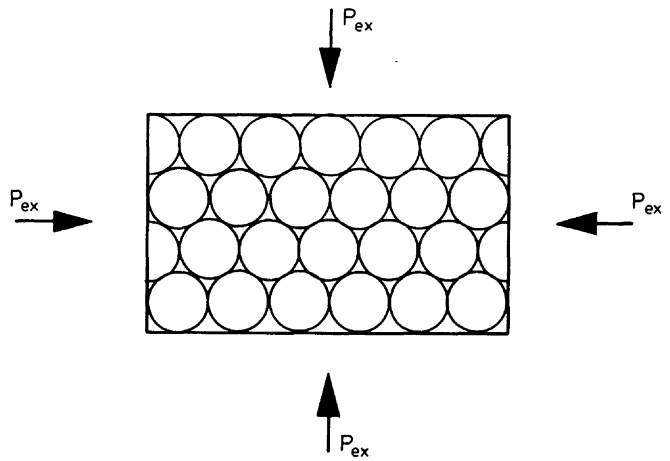

FIG. 3. A schematic diagram of hexagonal array of cylinders subjected to an external hydrostatic loading P_{ex}.

the deformation characteristics of plasticene are similar to those of metals, and plasticene therefore serves as a good model material.

2. GEOMETRICAL RELATIONSHIPS

In this section we develop equations for the relative density D (=density of porous solid/full density of solid constituent) of the hexagonally packed array of cylinders (Fig. 3) due to plastic flow. As in the densification of spherical particles we identify two stages of compaction: stages I and II. During the initial stage (stage I), the individual cylindrical particles are still recognizable and the pores remain cusped in shape. The densification in stage I is therefore modelled by the growth of particle–particle contacts. In the later stages of densification (stage II) the pores formed between the contacting particles are surrounded by a zone of plastically deforming material. It is now more instructive to model the geometry as an array of pores which shrink in size as the relative density of the compact increases. Two types of pore cross-sectional geometries are considered: circular and triangular. If densification occurs by plastic flow, as in cold compaction, the pores remain cusped, and the actual pore geometry is best approximated by a triangularly shaped pore. However, when the densification involves other mechanisms, such as diffusion, the pores can become rounded and a circularly cylindrical shape more closely approximates the actual pore geometry. We shall show that the pore geometry in stage II has a significant effect upon the densification process. First we discuss the particle geometry for the two stages of densification.

2.1. *The initial stage: stage I*

Consider a unit cell of the array consisting of a three-sided cusped pore within an equilateral triangular block of material of length $2y$, as shown in Fig. 4(a). Here $2y$ is the centre–centre distance of two contacting particles; $2y = 2R_0$ at the start of deformation, where R_0 is the initial particle radius, i.e. the particles are in point

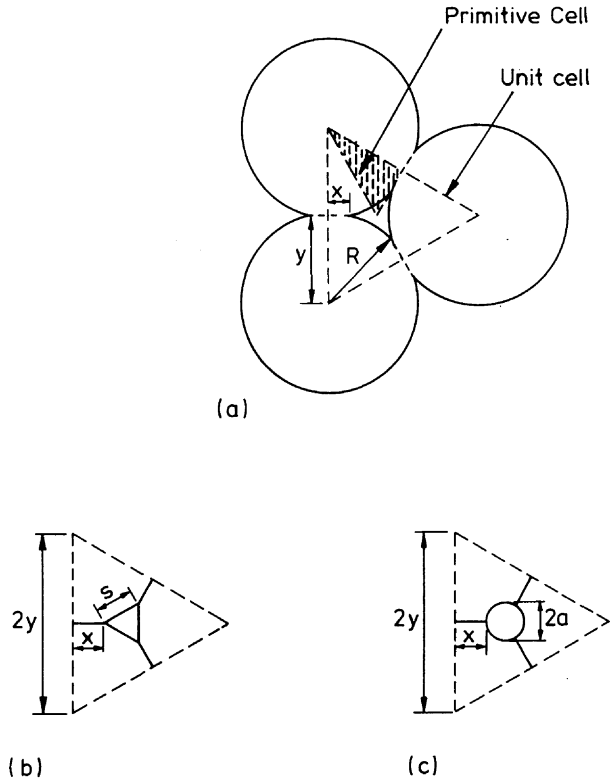

FIG. 4. The compaction of a hexagonal array of cylinders illustrating the unit cell. (a) The unit cell in stage I; the pore has a cusped shape. (b) The unit cell in stage II; the porosity has been approximated by a triangular pore of length s, and (c) the unit cell in stage II with a circularly cylindrical pore of radius a. In all cases, $2y$ is the particle centre–centre distance.

contact initially. We do not follow the evolution of the shape of the particle during the deformation process, but assume that at any instant during stage I the free surface of the pore can be represented by a circular arc of radius R with its centre of curvature coincident with the centre of the particle. Under a macroscopic hydrostatic loading in which the unit cell volume decreases, the particle centres move toward each other and contacts are formed between the particles. Deformation occurs in individual particles by radial flow of material into the void space along the axis of symmetry between two neighbouring contacts. This assumed mode of deformation ensures that the voids remain cusped; and is consistent with the observed void geometry in cold compaction and in the early stages of hot-isostatic pressing (SWINKEL *et al.*, 1983).

The contacts appear as flat rectangular faces on each particle; the contact size $2x$ is taken as the width of a rectangular face. The particle radius at any stage of the deformation, R, is related to the contact size $2x$ and the instantaneous centre–centre distance $2y$ by $R = (x^2+y^2)^{1/2}$. The volume of a unit length of a cylindrical particle at any stage of the deformation, V_p, is given by [see Fig. 4(a)]

$$V_p = \pi R^2 - Z(R^2\theta - xy), \tag{1}$$

where Z is the number of contacts per particle ($Z = 6$ for a close packed array of rods), and $\theta = \tan^{-1}(x/y)$. By equating V_p to the initial volume of a unit length of the particle $V_o = \pi R_o^2$ (R_o is the radius of the particle at zero deformation), we obtain

$$\frac{R}{R_0} = \left\{1 - \frac{Z}{\pi}\left[\tan^{-1}\left(\frac{x}{y}\right) - \left(\frac{x}{y}\right)^{-1}\left[1 + \left(\frac{x}{y}\right)^{-2}\right]^{-1}\right]\right\}^{-1/2}. \quad (2)$$

The relative half contact size x/y varies from a value of $x/y = 0$ at the start of densification to a value of $x/y = 1/\sqrt{3}$ at full density. Figure 5 shows a plot of R/R_0 against x/y; $R \approx R_0$ for $x/y \leqslant 0.1$.

The relative density D is defined as the ratio of the volume of material in a unit cell to the total volume of the unit cell. For the unit cell shown in Fig. 4(a), the relative density D can be shown to be

$$\frac{D}{D_0} = \left(\frac{R}{R_0}\right)^{-2}\left(1 + \frac{x^2}{y^2}\right), \quad (3a)$$

where $D_0 = 0.906$ is the value of D at $x/y = 0$. For values of x/y in the range $0 < x/y \leqslant 0.3$, the expression for the relative density given by (3a) can be approximated by a linear relationship

$$\frac{D}{D_0} = 1 + \frac{3}{20}\frac{x}{y}, \quad (3b)$$

which is within $\pm 0.5\%$ of the exact solution.

2.2. *The final stage: stage II*

During the final stage, the pores are idealized as regularly spaced holes surrounded by plastically deforming material. Two pore geometries are considered: triangular and circular cylindrical pores. The unit cell for each pore geometry is chosen to be representative of that for the whole compact.

The unit cell for the triangular pore is similar to that shown in Fig. 4(a) but with the cusped shaped pore in stage I replaced by an equilateral triangular pore of length

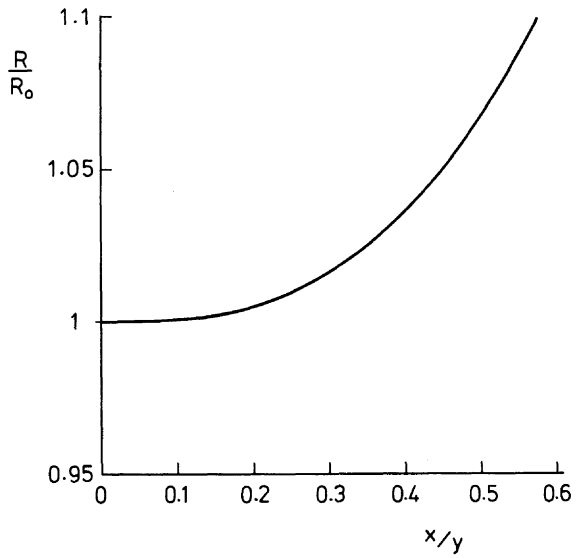

FIG. 5. The normalized instantaneous particle radius R/R_0 as a function of normalized half contact size x/y. R_0 is the initial particle radius and $2y$ is the particle centre–centre distance.

s, as shown in Fig. 4(b). Straightforward geometrical considerations give the relative size of the triangular pore s/y in terms of the relative contact size x/y,

$$\frac{x}{y} = \frac{1}{\sqrt{3}}\left(1 - \frac{s}{y}\right). \tag{4}$$

The relative density D is now given by

$$D = 1 - \frac{1}{4}\left(1 - \sqrt{3}\frac{x}{y}\right)^2. \tag{5}$$

The unit cell when the pores are circular [Fig. 4(c)] consists of a circular pore of radius a within a deforming equilateral triangular block of length $2y$. The relative pore radius a/y is related to the relative contact size x/y by

$$\frac{x}{y} = \frac{1}{\sqrt{3}} - \frac{a}{y} \tag{6}$$

and the relative density D is given by

$$D = 1 - \frac{\pi}{3\sqrt{3}}\left(1 - \sqrt{3}\frac{x}{y}\right)^2. \tag{7}$$

The size of both the triangular pore, s, and the radius of the cylindrical pore, a, decrease with increasing densification: both s/y and a/y vanish as full density ($D = 1$) is approached.

Previous material models for stage II densification assume a unit cell which consists of a circularly cylindrical pore surrounded by a cylindrical shell of material. We shall show in the following section that the slip-line field solution within the plastically deforming region around each cylindrical pore is the same as that given by the thick-walled cylinder model.

3. DENSIFICATION PRESSURE: SLIP-LINE FIELD APPROACH

3.1. *Stage I*

If the cylindrical particles are free to slide on each other so that the contact surface cannot support any shear stresses, the deformation can be modelled by considering the indentation of a long cylindrical material by a smooth rigid flat punch. The material is assumed to be rigid and perfectly plastic, and the length of the cylinder is assumed to be much greater than the diameter so that a plane strain analysis is applicable.

For the hexagonal array of cylinders, the deformation is modelled by six equally spaced smooth, rigid flat punches of equal width indenting a rigid–perfectly plastic cylinder. Slip-line field theory (HILL, 1950) is used to evaluate the indentation pressure. When the externally applied loading P_{ex} is hydrostatic (as shown in Fig. 3) symmetry conditions dictate that only 1/12 of the cylinder needs to be considered (the primitive cell of Fig. 4). Typical slip lines for the indented cylinder are shown in Fig. 6, with

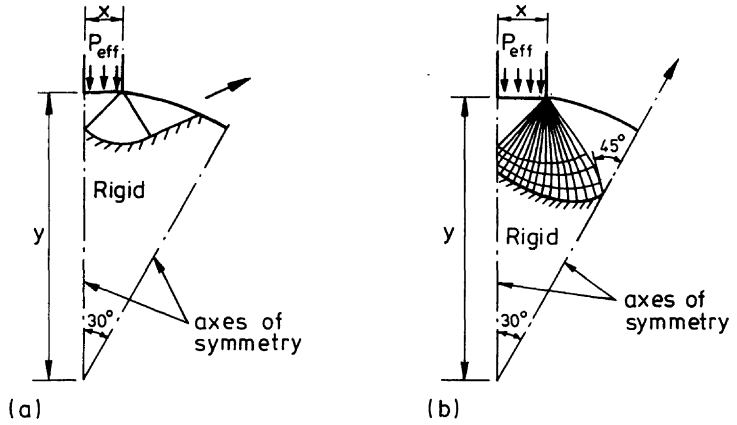

FIG. 6. The slip-line fields for stage I. (a) Isolated contact, and (b) contact–contact interaction.

displacement of the material occurring symmetrically about the punch during the indentation.

At the start of densification, when the contacts are much smaller than the particle radius, the deformation is localized and there is no interaction between the contacts. The slip lines at this stage are Prandtl fields (HILL, 1950), see Fig. 6(a). The field assumes a triangular zone of dead material adheres to the punch and moves as a rigid body with the punch. The uniform pressure P_{eff} on the flat punch, neglecting the small curvature of the particle, is $P_{eff} = [(2+\pi)/\sqrt{3}]\sigma_y = 2.97\sigma_y$, where the material is assumed to obey Von Mises yield condition and σ_y is the uniaxial yield stress of the material composing the cylindrical particles.

As densification progresses and the contact size increases, the distance between neighbouring contacts decreases and the contacts begin to interact when the contact size is no longer small compared with the distance between the contacts. Typical slip line fields when the contacts interact with each other are shown in Fig. 6(a). A triangular zone of dead material is attached to the punch surface and the nets of orthogonal slip lines starting from the corner of the punch intersect the axes of symmetry at 45° (JOHNSON, 1958). The material in the centre of the indented cylinder is rigid while that on the outer side of the slip lines moves as a rigid body outward along the axis of symmetry with progressive deformation. The uniform pressure P_{eff} on the punch surface is evaluated using Hencky's equations and the condition that the net force on the zone of dead material along the axis of symmetry between neighbouring punches is zero. The pressure P_{eff} is given by $P_{eff} = c(x/y)\sigma_y$ for the case of contact–contact interaction, where c is a dimensionless function of x/y, and $c \leqslant 2.97$. Thus, the interaction between contacts results in a net softening of the material response.

The transition from the case of isolated contacts to that of contact–contact interaction occurs when the slip-line field of Fig. 6(b) provides a value of P_{eff}/σ_y equal to the Prandtl value of 2.97. Based on this condition, we note that the transition occurs at a value of $x/y \approx 0.1$. The slip-line field of Fig. 6(b) is admissible provided the angle between the outermost slip line emanating from the corner of the punch and the stress-free particle surface is greater than or equal to 45° (JOHNSON *et al.*, 1970). We observe that this condition is satisfied for values of $x/y \leqslant 0.27$. In the current paper we identify the condition where $x/y = 0.27$ as the end of stage I. We therefore

conclude (based upon the assumed mode of deformation shown in Fig. 6) that stage I densification terminates at $x/y = 0.27$, which corresponds to a relative density of $D = 0.95$.

Figure 7 shows the normalized contact pressure (or inter-particle pressure) P_{eff}/σ_y as a function of the relative contact size x/y; $P_{\text{eff}}/\sigma_y = 2.97$ for $x/y \leqslant 0.1$ (isolated contact) and it decreases with increasing contact size to a value of $P_{\text{eff}}/\sigma_y = 2.36$ at $x/y = 0.27$, due to particle contact–contact interaction. We observe that the isolated contact model considerably overestimates the inter-particle mean contact pressure P_{eff} for values of relative contact size x/y in the range $0.1 < x/y \leqslant 0.27$ (i.e. $0.915 < D \leqslant 0.95$). The results of P_{eff}/σ_y in the range $0.1 < x/y \leqslant 0.27$ can be fitted to a function of the form

$$\frac{P_{\text{eff}}}{\sigma_y} = \frac{6}{5}\left(\frac{D-D_o}{D_o}\right)^{-1/5}, \tag{8}$$

which is within $\pm 5\%$ of the slip-line field solution. The relative density D is related to the relative contact size x/y as given by (3) and D_o ($=0.906$) is the initial relative density. A variety of more accurate functions can be fitted to the slip-line field solution; such functions are, in general, complex and difficult to use. In the present study, we assume the function given by (8) gives a reasonable description of the slip-line field solution especially when many material properties (for example, the yield stress and the strain hardening exponent) can only be measured to within 20% of their actual values.

3.2. *Stage II*

The three-sided cusped pore at the end of stage I is approximated firstly by a triangular pore, and secondly by a circular pore. First we discuss the fields for the

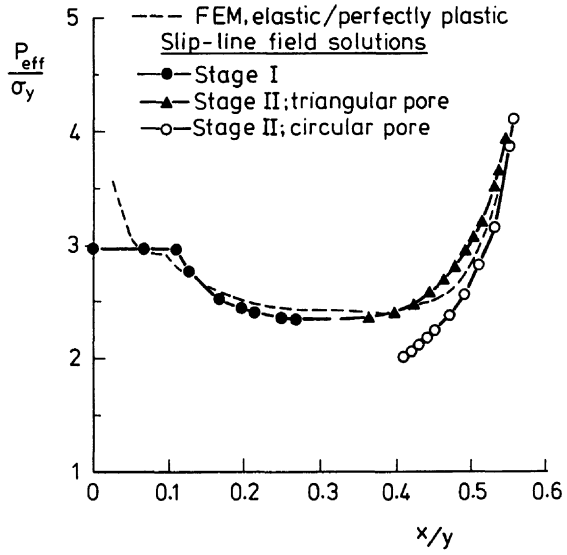

FIG. 7. The effect of relative contact size x/y on the normalized mean contact pressure P_{eff}/σ_y. The finite element results are for elastic–perfectly plastic material with $\sigma_y/E = 10^{-4}$, where σ_y is the yield stress of the material and E the Young's modulus.

triangular pore. The slip-line field is shown in Fig. 8(a). A triangular zone of dead material is attached to the surface of the triangular pore and the centre-fan field is extended to intersect the contact surface and the axis of symmetry between the contacts at 45°. The deformation is therefore localized around the pore and the contact, and a rigid region exists at the centre of the particle. The mode of deformation shown in Fig. 8(a) is strictly valid for values of half contact size, x, greater than or equal to the triangular pore size, s. Geometric considerations dictate that the assumed field is valid for $x/y \geqslant 0.37$, i.e. for $D \geqslant 0.966$. Recall that the slip-line field of Fig. 6(b) is only valid for $D \leqslant 0.95$. We therefore regard the region $0.95 < D < 0.966$ as the interval of transition from stage I to stage II; the precise mode of deformation in this interval is yet to be determined.

In contrast with the stage I behaviour, the normal pressure on the contact surface is not uniform across the contact. In presenting the results for the contact pressure, P_{eff} is taken as the average normal pressure over the contact surface. The normalized average pressure P_{eff}/σ_y on the contact surface is included in Fig. 7 as a function of the relative contact size x/y; P_{eff}/σ_y increases with x/y and an infinite value of P_{eff}/σ_y is required to attain full density ($x/y = 1/\sqrt{3}$ at full density). An empirical fit to the

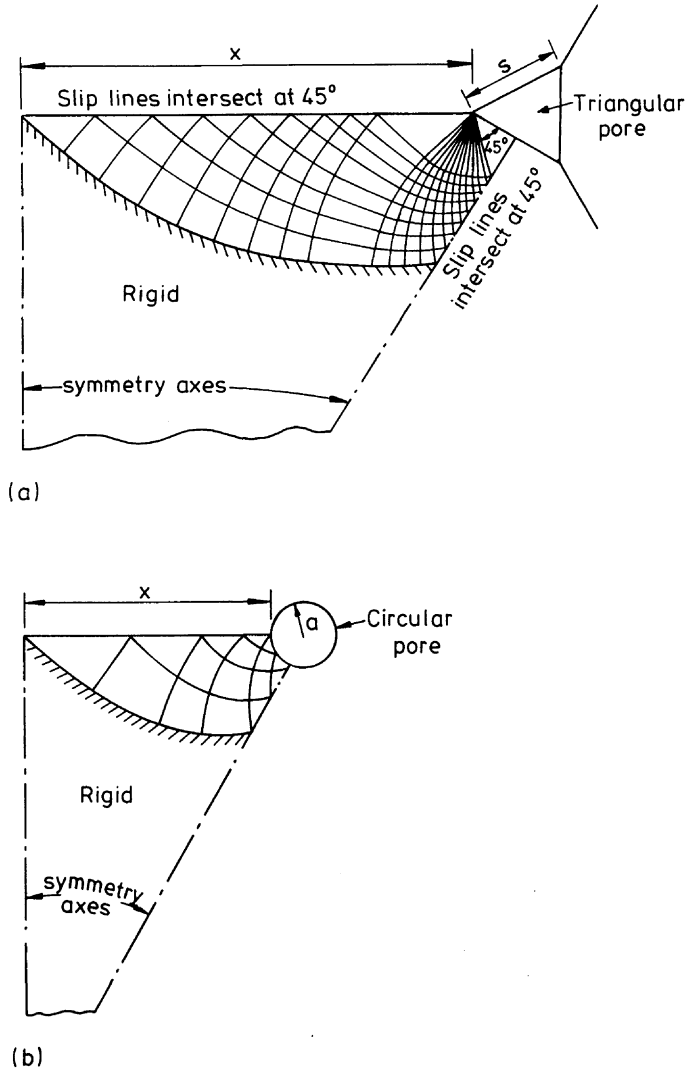

FIG. 8. The slip-line fields for stage II. (a) Triangular pore geometry, and (b) circular pore geometry.

results for the triangular pore plotted in Fig. 7 is given by

$$\frac{P_{\text{eff}}}{\sigma_y} = 0.6[1-2(1-D)^{1/2}]^{-3/2} \ln\left(\frac{1}{4(1-D)}\right), \tag{9}$$

which is within $\pm 1\%$ of the slip-line field solution. The relative density D is given as a function of x/y by (5).

Now consider the case of a circular pore of radius a surrounded by an equilateral triangular block of length $2y$. The slip lines for the circular pore geometry are logarithmic spirals, and are shown in Fig. 8(b). As in the case of a triangular pore, the deformation is concentrated around the pore and the contact surface; the centre of the particle remains rigid. There is an overlapping of the slip-line fields of two neighbouring pores on the contact surface to account for the effect of void–void interaction. The stress field in the plastically deforming region is similar to that in a thick-walled cylinder. The traction where the slip line meets the contact surface is purely normal and is determined analytically from the equilibrium equation for a thick-walled cylinder, and the yield condition:

$$\sigma_{\theta\theta} = \frac{2\sigma_y}{\sqrt{3}}\left[1+\ln\left(\frac{r}{a}\right)\right], \tag{10}$$

where r is the radial distance from the centre of the pore. Thus, the normal pressure $\sigma_{\theta\theta}$ varies over the contact. By writing P_{eff} as the average normal pressure over the contact, we have for the circular pore

$$P_{\text{eff}} = \frac{1}{x}\int_a^{a+x} \sigma_{\theta\theta}\,\mathrm{d}r = \frac{\sigma_y}{\sqrt{3}}\left[1-3\left(\frac{1-D}{\pi}\right)^{1/2}\right]^{-1} \ln\left(\frac{\pi}{3\sqrt{3}(1-D)}\right), \tag{11}$$

where D is given as a function of x/y by (7). P_{eff}/σ_y is plotted in Fig. 7 as a function of x/y for the circular pore; P_{eff}/σ_y increases with x/y and an infinite value of P_{eff}/σ_y is required to attain full density, as in the case of a triangular pore geometry. When employing this geometric description of the circular pore we assume, as before, that (8) for stage I is valid for $D \leqslant 0.95$, so that (11) is valid for values of D greater than this.

3.3. *Density–pressure relationship for stage I and stage II*

If we assume that the mean contact pressure P_{eff} is equivalent to the inter-particle pressure, equilibrium dictates that the macroscopic hydrostatic loading P_{ex} applied to the hexagonal array of cylinders (Fig. 3) be related to P_{eff} by

$$P_{\text{ex}} = \sqrt{3}\frac{x}{y}P_{\text{eff}}, \tag{12}$$

where $2x$ is the contact size and $2y$ is the particle centre–centre distance. In stage I, $P_{\text{eff}} = 2.97\sigma_y$ for isolated contacts, $x/y \leqslant 0.1$ (i.e. $D \leqslant 0.915$) and P_{eff} is given as a function of D by (8) for the case of contact–contact interaction. The mean contact pressure P_{eff} in stage II is given as a function of D by (9) for the triangular pore and

by (11) for the circular pore. The relative density D is related to the relative contact size x/y by (3), (5) and (7). Thus, we can determine the macroscopic pressure P_{ex} as a function of the relative density D by using (12). In each case

$$P_{ex} = f(D)\sigma_y, \tag{13a}$$

where

$$f(D) = \begin{cases} 2.97\left[\dfrac{3(D-D_o)}{D_o}\right]^{1/2} & D \leqslant 0.915, \text{ for isolated contacts in stage I} \\ 8\sqrt{3}\left(\dfrac{D-D_o}{D_o}\right)^{4/5} & 0.915 < D \leqslant 0.95, \text{ for contact–contact interaction in stage I} \\ 0.6[1-2(1-D)^{1/2}]^{-1/2} \ln\left(\dfrac{1}{4(1-D)}\right) & D \geqslant 0.966, \text{ for the triangular pore in stage II} \\ \dfrac{1}{\sqrt{3}} \ln\left(\dfrac{\pi}{3\sqrt{3}} \dfrac{1}{(1-D)}\right) & D \geqslant 0.95, \text{ for the circular pore in stage II.} \end{cases} \tag{13b}$$

Figure 9 shows the normalized external hydrostatic pressure P_{ex}/σ_y as a function of the relative density D. An infinite external pressure is required for both the triangular and the circular pore geometries to attain full density. The results show that the triangular pore is more compressible than the circular pore at lower values of D. This is consistent with previous theoretical and numerical studies on the compressibility of pores (ZIMMERMAN, 1986; O'DONNELL and STEIF, 1989). Also, the detailed distribution of porosity has a strong influence on the material response. The pressure–density curves for the two pore geometries nearly converge as full density is approached. Conventional models of stage II compaction, which employ a thick-

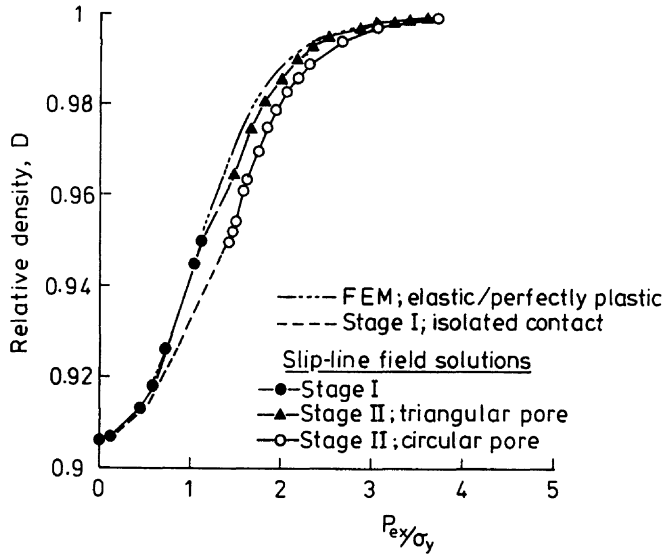

FIG. 9. The normalized macroscopic hydrostatic pressure P_{ex}/σ_y as a function of the relative density D.

walled cylindrical (or spherical) shell as a unit cell, assume that the entire body deforms plastically as it densifies. With the more realistic arrangement of voids and selection of unit cell considered here, it is found that a large central region of a particle remains rigid with deformation confined to a band of material around the circumference of the particle. This, combined with a more accurate description of the pore shape, results in a smoother transition from stage I to stage II than conventional models, and in a much higher compressibility. It is further evident from the results plotted in Fig. 9 that the isolated contact model considerably overestimates the macroscopic hydrostatic pressure required to attain a given density. For example, at a relative density of 0.95, the isolated contact model overestimates the macroscopic hydrostatic yield pressure by about 25%.

4. EFFECT OF MATERIAL STRAIN HARDENING: FINITE ELEMENT STUDY

Finite element analyses were carried out to investigate the effect of material strain hardening, and to supplement the slip-line field solutions discussed above. Due to the symmetry of the problem, we consider only a 30° segment of the circular particle as shown for example in Fig. 6(a). The finite element mesh contains approximately 444 8-noded plane strain elements. A uniform displacement is applied to the flat rigid punch which is free to slide on the contact surface. The symmetry planes are constrained to have zero-normal velocity and the results are obtained for finite strain deformation theory as implemented in ABAQUS† finite element code.

For comparison purposes, solutions were obtained for an elastic–perfectly plastic material. The elastic strain is chosen to be very small so as to mimic a rigid–perfectly plastic behaviour, $\sigma_y/E = 10^{-4}$, where σ_y is the uniaxial yield stress of the material, E is Young's modulus and Poisson's ratio $\nu = 0.33$. The finite element calculations give the half contact size, x, the half centre–centre distance, y, and the average normal pressure over the contact, P_{eff}, as a function of the depth of punch indentation.

Figure 10 shows the variation of the normal pressure along the contact surface for selected values of relative contact size x/y. Slip-line field solutions suggest the normal pressure in stage I ($x/y \leqslant 0.27$) is uniform over the contact surface. However, we observe a slight numerical oscillation in the values of the normalized normal pressure P_{eff}/σ_y over the punch surface evaluated by the finite element method for $x/y \leqslant 0.27$ [see Fig. 10(a)]. For a given calculation, the value of the normal contact pressure P_{eff} reported for the finite element analysis both in stage I and in stage II is the average of the normal pressure over the whole contact surface. The variation of the normal pressure over the contact surface in stage II as predicted by the slip-line field analysis is in close agreement with the prediction from the finite element analysis for the triangular pore, see Fig. 10(b).

The results of P_{eff}/σ_y versus x/y for the elastic–perfectly plastic material are included in Fig. 7; there is good agreement between the finite element solutions and the slip-line field solutions. The initial high value of P_{eff}/σ_y for the finite element analysis is attributed to the elastic response while the slightly lower value of P_{eff}/σ_y in the isolated

† HIBBITT, KARLSSON and SORENSON (1984).

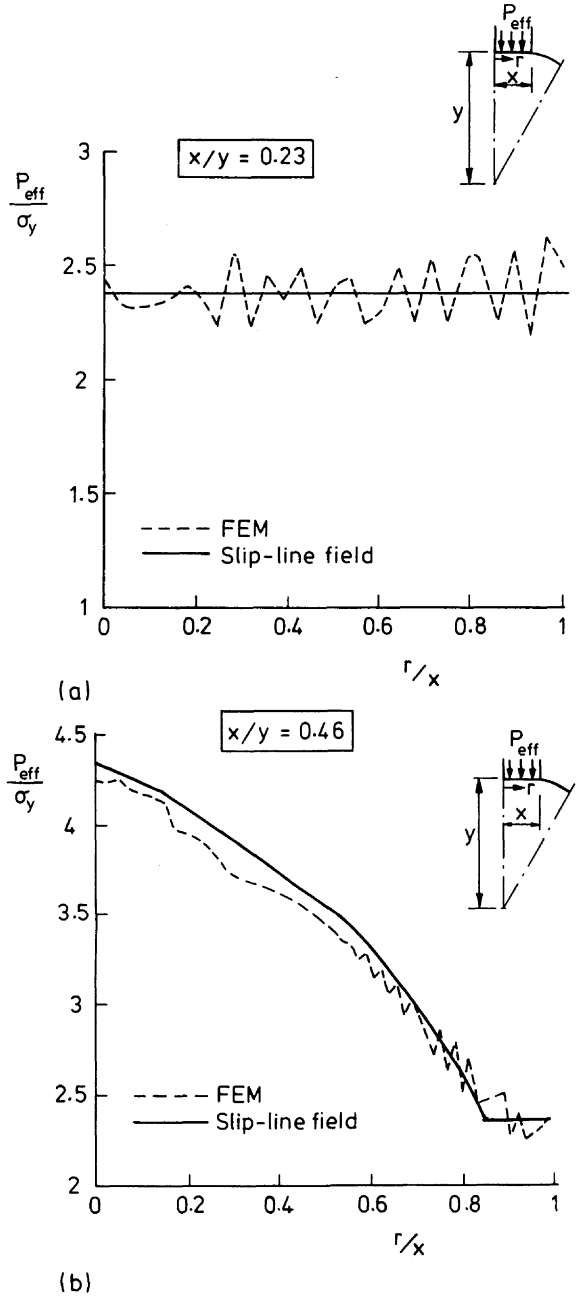

FIG. 10. The variation of the normal pressure P_{eff} on the contact surface with distance r from the punch axis of symmetry. The normal pressure has been normalized by the yield stress of the material, σ_y, and the distance r has been normalized by the half contact size x. (a) $x/y = 0.23$ and (b) $x/y = 0.46$, where $2y$ is the particle centre–centre distance.

contact region ($x/y \leqslant 0.1$) is attributed to the curvature of the particle, which was neglected in the slip-line field analysis. The external pressure P_{ex}, versus relative density D, from the finite element analysis is plotted in Fig. 9. Again there is good agreement between the slip-line field and finite element solutions. The stage II solutions from the finite element analysis are in closer agreement with the slip-line field solutions for the triangular pore than with those for the circular pore. This suggests that the approximation of the pore geometry as triangular is a fairly good one, since the finite

element analysis maintains the cusped shape of the pore; typical pore shapes are shown in Fig. 11.

In order to investigate the effect of material strain hardening, we consider a Ramberg–Osgood deformation theory solid with a constitutive relation

$$\frac{\varepsilon}{\varepsilon_y} = \frac{\sigma}{\sigma_y} + \alpha\left(\frac{\sigma}{\sigma_y}\right)^{1/N}, \tag{14}$$

where σ_y is the initial yield stress corresponding to a yield strain $\varepsilon_y = \sigma_y/E$, E is Young's modulus, α is a dimensionless constant and N is the strain hardening exponent with a value in the range $0 \leqslant N \leqslant 1$. For very small values of N, the plastic strain remains small until σ exceeds σ_y. In the limit $N = 0$, (14) describes an elastic–perfectly plastic solid. For all the cases considered in the present analysis, the value of the dimensionless constant α was chosen such that $\sigma = \sigma_y$ is the flow stress at an offset strain ε_{off} $(=\alpha\varepsilon_y)$ of 0.1%.

The external pressure versus density response for $\varepsilon_y = 10^{-4}$ and for various values of the strain hardening exponent N is shown in Fig. 12. The external pressure P_{ex} has been normalized by the initial yield stress, σ_y. The compressibility of the array decreases with increasing value of the strain hardening exponent.

A further study was carried out to examine the effect of the initial yield strain

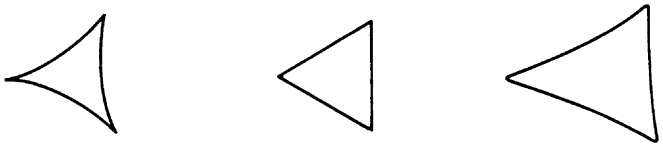

F. E. M. Slip-line field Experiment

FIG. 11. Schematic of typical pore shapes at a relative density $D = 0.983$.

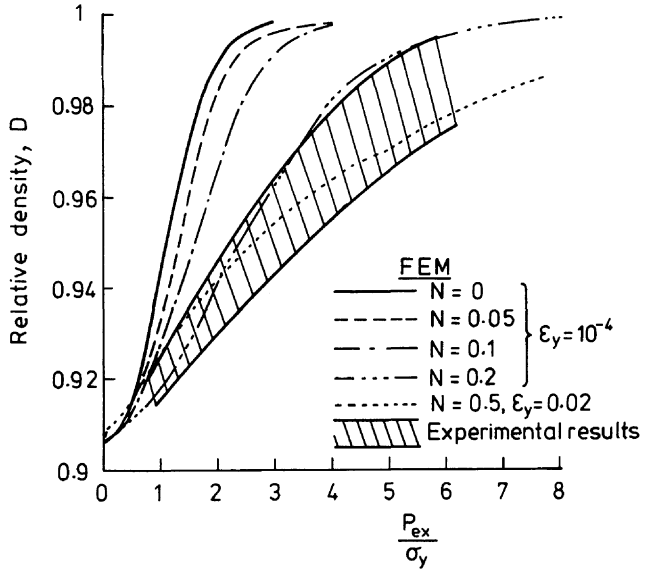

FIG. 12. The effect of material strain hardening exponent N upon the density–external pressure curves. $\sigma_y/E = 10^{-4}$ where σ_y is the yield stress at 0.1% offset strain. The experimental results are for the hydrostatic compaction of plasticene cylinders; $N = 0.5$ and $\sigma_y/E = 0.02$ for plasticene.

$\varepsilon_y = \sigma_y/E$ upon the densification process. We find no effect of the initial yield strain on the pressure–density response for $N = 0.1$ and $10^{-4} \leqslant \varepsilon_y \leqslant 0.005$. Previous studies of compaction of a hexagonal array of cylinders using a linear hardening constitutive relation showed a significant effect of the initial yield strain on the pressure–density response. In particular, the finite element solutions of O'DONNELL and STEIF (1989) showed an increasing compressibility of the array with decreasing values of the initial yield strain. The difference between the present results and those of O'DONNELL and STEIF (1989) suggest the possibility that the pressure versus density response is dependent upon the particular form of constitutive relation used.

5. COMPARISON WITH EXPERIMENTS

Hydrostatic compaction tests were performed on a hexagonal array of plasticene cylinders, in order to compare with the predictions of the finite element analysis. First, uniaxial compression tests were performed on plasticene cylinders at room temperature in order to measure the material properties. The cylinders used for the uniaxial test were of diameter 15 mm and of length 25 mm. The nominal stress–strain curves are shown in Fig. 13; the cylinders deformed by localized shear. The 0.1% offset yield stress of the plasticene σ_y is 0.08 MPa at a nominal strain rate of 7×10^{-4} s^{-1}. For straining beyond $\varepsilon_y \approx 0.02$, the true stress ($\sigma$) versus true strain ($\varepsilon$) curve of the cylinder can be described by a power law $\sigma = A\varepsilon^{0.5}$, where $A = 0.66 \pm 0.03$ MPa. Thus, the plasticene exhibits appreciable strain hardening.

Hydrostatic compaction tests were performed on the hexagonal array of plasticene cylinders using an isostatic cell, with water as the pressurizing medium. Plasticene cylinders of length 76 mm and of diameter 5 mm were made by extrusion, and left for about a week to age at room temperature. The surface of the cylinders was coated with talcum powder to allow them to slide with respect to each other, and arranged in a close-packed form inside a thin flexible rubber membrane. The array had an initial average diameter of about 38 mm. The flexible membrane containing the

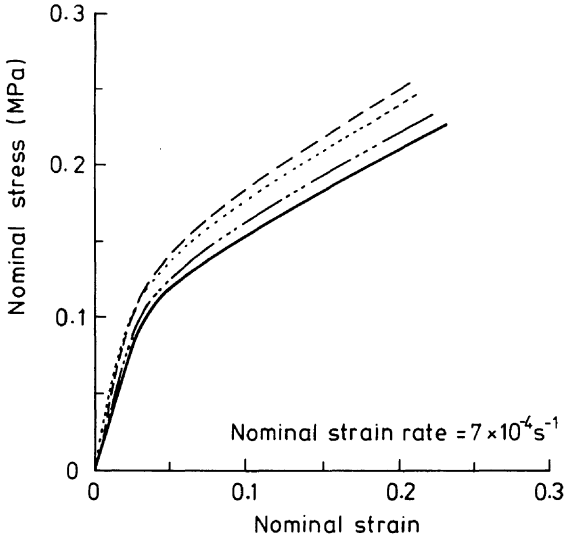

FIG. 13. The uniaxial stress–strain curves in compression for plasticene. The tests were conducted at room temperature ($\approx 20°C$) and at a nominal strain rate of 7×10^{-4} s^{-1}.

cylindrical particles was carefully placed inside the cell and pressurized to a set value of pressure. Each pressure was held for about 5 min and then removed. The diameter of the array after the pressure had been applied was measured at six different points along the length of the array. The relative density was evaluated from the ratio of the volume of solid cylinder in the array to the total volume (including void spaces) of the array. The length of the array remained approximately constant; the maximum contraction was less than 1% of the initial value.

The scatter band in measured P_{ex}/σ_y versus D response is shown in Fig. 12: data are from three nominally identical tests. The upper limit of the experimental results is approximately along the finite element prediction for particles with a strain hardening exponent $N = 0.2$ and a yield strain $\varepsilon_y = 10^{-4}$, while the finite element predictions for $N = 0.5$, $\varepsilon_y = 0.02$ lie within the band. The wide range in the experimental results between a strain hardening exponent $N = 0.2$ and $N = 0.5$ is in agreement with previously determined values of N for plasticene. The strain hardening exponent N was found to have a value of $N = 0.21$ by CHIJIIWA *et al.* (1980) and $N = 0.35$ by MCCLINTOCK (1968); the uniaxial test on the plasticene used for the present study gave a value of $N = 0.5$. The deformation characteristics of plasticene are, however, very sensitive to slight changes in temperature and moisture content. We conclude that the experimentally measured values of the macroscopic yield pressure for hydrostatic compaction of the cylindrical plasticene particles are in fair agreement with the theoretical predictions to within the range of values of the strain hardening exponent quoted in the literature.

The typical shape of a pore in stage II is compared with that obtained from the finite element analysis and the assumed shape in the slip-line field study in Fig. 11. It is interesting to note that the actual shape is closer to the triangular form assumed in the slip-line field analysis than that obtained from the finite element simulation. This observation further supports the view that the assumption of a triangular shaped pore adequately models the stage II response.

6. CONCLUDING DISCUSSION

The results of the slip-line field and finite element calculations indicate that interaction between contacts and pore shape influence the pressure–density relationship of a regular array of cylinders. The simplifications used in the present study do not allow us to address the features arising from particle rearrangement. The cusp-shaped pore, which is typical of the cold compaction of powders, can be modelled reasonably well by a triangularly-shaped pore. Circularly cylindrical pores give a stronger macroscopic response than triangularly shaped ones.

In this paper, we have examined the role of contact–contact interaction on the densification of cylindrical particles by hydrostatic loading. Deviatoric stressing results in shape change and in unequal contact sizes. The role of deviatoric stressing in the densification of spherical powders has been explored in a separate study by FLECK *et al.* (1990) using an isolated contact model. The modelling of the effect of contact–contact interaction in the presence of deviatoric stress is in progress.

Acknowledgements

This work was supported by a contract (N00014-91-J-4089) with the Defense Advanced Projects Agency and the Office of Naval Research through a collaborative programme with the University of Virginia. Fruitful discussions with Profs M. F. Ashby and H. Wadley are gratefully acknowledged.

References

Arzt, E. (1982) The influence of an increasing particle coordination on the densification of spherical powders. *Acta Metall.* **30,** 1881–1890.

Ashby, M. F. (1990) *Background Reading: Hot Isostatic Pressing and Sintering.* Internal Report, Cambridge University Engineering Department, Cambridge.

Chijiiwa, K., Hatamura, Y. and Hasegawa, N. (1980) Characteristics of plasticene used in the simulation of slab in rolling and continuous casting. *Trans. Iron and Steel Inst. of Japan* **21,** 48–57.

Fleck, N. A., Kuhn, L. T. and McMeeking, R. M. (1990) Yielding of metal powder bonded by isolated contacts. *J. Mech. Phys. Solids* **40,** 1139–1162.

Helle, H. S., Easterling, K. E. and Ashby, M. F. (1985) Hot-isostatic pressing diagrams: new developments. *Acta Metall.* **33,** 2163–2174.

Hill, R. (1950) *Mathematical Theory of Plasticity.* Oxford University Press, Oxford.

Johnson, W. (1958) Indentation and forging and the action of Nasmyth's anvil. *The Engineer* **205,** 340–350.

Johnson, W., Sowerby, R. and Haddow, J. D. (1970) *Plane-strain Slip-line Fields: Theory and Bibliography.* Edward Arnold (Pub.) Ltd.

Kakar, A. K. and Chaklader, A. C. D. (1967) Deformation theory of hot-pressing. *J. Appl. Phys.* **38,** 3223–3230.

Liu, Y.-M., Wadley, H. N. G. and Duva, J. (1993) Densification of porous materials by power-law creep. To be published.

Matsumura, G. (1971) Sintering of iron wires. *Acta Metall.* **19,** 851–855.

McClintock, F. A. (1968) A criterion for ductile fracture by the growth of holes. *J. Appl. Mech.* **35,** 363–371.

O'Donnell, T. P. and Steif, P. S. (1989) Elastic–plastic compaction of two-dimensional assemblage of particles. *J. Engng Mater. Technol.* **111,** 404–408.

Swinkel, F. B. and Ashby, M. F. (1981) A second report on sintering diagrams. *Acta Metall.* **29,** 259–281.

Swinkel, F. B., Wilkinson, D. S., Arzt, E. and Ashby, M. F. (1983) Mechanisms of hot-isostatic pressing. *Acta Metall.* **31,** 1829–1840.

Williamson, R. L., Knibloe, J. R. and Wright, R. N. (1992) Particle-level investigation of densification during uniaxial hot pressing: continuum modeling and experiments. *J. Engng Mater. Technol.* **114,** 105–110.

Zimmerman, R. W. (1986) Compressibility of two-dimensional cavities of various shapes. *J. Appl. Mech.* **53,** 500–504.